Interaction of a 180° ferroelectric domain wall with a biased scanning probe microscopy tip: Effective wall geometry and thermodynamics in Ginzburg-Landau-Devonshire theory

Anna N. Morozovska,[1,*] Sergei V. Kalinin,[2,†] Eugene A. Eliseev,[3] Venkatraman Gopalan,[4] and Sergei V. Svechnikov[1]
[1]*Institute of Semiconductor Physics, 41, pr. Nauki, 03028 Kiev, Ukraine*
[2]*The Center for Nanophase Materials Sciences and Materials Science and Technology Division, Oak Ridge National Laboratory, Oak Ridge, Tennessee 37831, USA*
[3]*Institute for Problems of Materials Science, National Academy of Science of Ukraine, Krjijanovskogo 3, 03142 Kiev, Ukraine*
[4]*Department of Materials Science and Engineering, Pennsylvania State University, University Park, Pennsylvania 16802, USA*
(Received 15 June 2008; revised manuscript received 10 August 2008; published 12 September 2008)

The interaction of ferroelectric 180°-domain wall with a strongly inhomogeneous electric field of biased scanning probe microscope tip is analyzed within continuous Ginzburg-Landau-Devonshire theory. Equilibrium shape of the initially flat domain-wall boundary bends, attracts, or repulses from the probe apex, depending on the sign and value of the applied bias. For large tip-wall separations, the probe-induced domain nucleation is possible. The approximate analytical expressions for the polarization distribution are derived using direct variational method. The expressions provide insight into how the equilibrium polarization distribution depends on the wall finite width, correlation and depolarization effects, electrostatic potential distribution of the probe and ferroelectric material parameters.

DOI: 10.1103/PhysRevB.78.125407 PACS number(s): 77.80.Fm, 77.22.Ej

I. INTRODUCTION

Domain-wall motion in disordered media is one of the fundamental mechanisms that control order-parameter dynamics in ferroelectric and ferromagnetic materials. The interplay between wall stiffness, driving force, pinning, and thermal excitations gives rise to a broad spectrum of remarkable physical phenomena including transitions between pinned, creep, and sliding regimes, dynamic phase transitions, and self-organized critical behavior. This behavior controlled by *homogeneous* external electric field was studied in details both experimentally and theoretically.[1–4] In most experimental studies to date, the domain-wall dynamics is inferred from the macroscopic response of the system to macroscopic field detected through changes in polarization, ac susceptibility, lattice parameters, and pyroelectric, piezoelectric, and optical properties. Recently, the *local* observations of domain-wall geometry and its evolution in uniform external fields have allowed direct information on static wall structure formed after field application, dynamic avalanche time and size distributions, and pinning on individual defects.[5–7]

The emergence of the scanning-probe-microscopy (SPM)-based techniques in the last decade opens the pathway to concentrate electric field within a small (~10–100 nm) volume of material. Combined with electromechanical response detection, this piezoresponse force microscopy (PFM) approach has been broadly applied for domain imaging and polarization patterning. Piezoresponse force spectroscopy was used to study polarization switching in the small volumes with negligible defect concentration,[8] map distribution of random bond and random field components of disorder potential,[9] and map polarization switching on a single defect center.[10] These experimental developments have been complemented by the extensive theoretical analysis of domain nucleation mechanisms in the SPM field probe on the ideal surface[11–13] and in the presence of charged defects in the rigid ferroelectric approximation (abrupt domain walls).[14] Recently, phase-field and analytical models have emerged to treat this problem in the framework of Ginzburg-Landau-Devonshire (GLD) theory (diffuse walls).[15] Here, we develop the analytical theoretical model for the interaction of the biased SPM probe and 180°-domain wall in the GLD model, paving the way for experimental studies of microscopic mechanisms of domain-wall polarization interaction with electric field that can be studied in strongly inhomogeneous fields of biased force microscope probe.

We note that this problem is similar to that of domain-wall pinning on a charged impurity, where the SPM probe acts as a "charged impurity" with controlled strength (controlled by tip bias) positioned at a given separation from domain wall. In this context, the problem of the infinitely thin ferroelectric domain-wall interaction with a charged point defect was considered by Sidorkin;[16] however, neither correlation effects (e.g., finite intrinsic width of domain walls) nor rigorous depolarization field influence were taken into account. For the description of domain-wall equilibrium position, the concept of Laplace tension (whose applicability to ferroelectrics has not been studied in detail) was used instead of the conventional GLD theory. Alternatively, thermodynamic Miller-Weinreich approach[1] or its combination with molecular-dynamics and Monte Carlo simulations as proposed by Rappe and co-workers[17] has been used. However, these models address domain-wall profile changes in homogeneous external field.

In this paper, we consider the interaction of ferroelectric 180°-domain-wall polarization with a strongly inhomogeneous electric field of biased force microscope probe within GLD thermodynamic approach. The nonlinear problem is resolved using direct variational method. The paper is organized as follows. The problem statement and basic equations are presented in Sec. II. In Sec. III we calculate the influence of the domain-wall finite width, correlation and depolarization effects, and ferroelectric material parameters on the

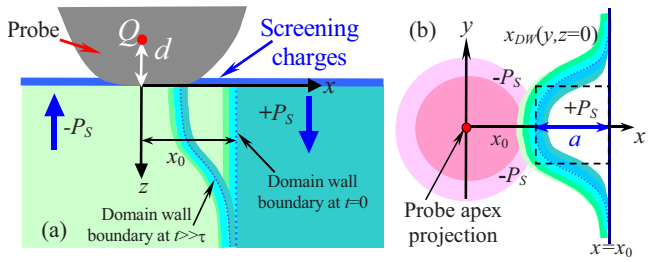

FIG. 1. (a) (Color online) Schematic of ferroelectric 180°-domain-wall boundary curved by the strong localized electric field of the biased probe in contact with the sample surface. (b) Wall curvature at the sample surface in quasicontinuous media approximation (solid curves and color scale). Dashed rectangle corresponds to the schematic of activation field calculations used by Miller and Weinreich (Ref. 1) for rigid polarization model where the distance a is equal to the lattice constant.

equilibrium domain-wall profile in the vicinity of biased probe. Coercive field for wall motion and domain nucleation is considered in Sec. IV. The results and implications for PFM studies of domain walls are discussed in Sec. V.

II. PROBLEM STATEMENT AND BASIC EQUATIONS

Here we consider the ferroelectric sample region that contains 180°-domain wall positioned in the vicinity of charged force microscope probe (Fig. 1). The region is free of lattice defects. Maxwell's equations for the inner electric field $\mathbf{E}(\mathbf{r},t)=-\nabla\varphi(\mathbf{r},t)$ expressed via electrostatic potential $\varphi(\mathbf{r},t)$ and polarization $\mathbf{P}(\mathbf{r},t)$ with boundary conditions are

$$\begin{cases} \mathrm{div}[\mathbf{P}(\mathbf{r},t)-\varepsilon_0\nabla\varphi(\mathbf{r},t)]=0, & z\geq 0, \\ \varphi(x,y,z=0,t)=V_e(x,y,t), & \varphi(x,y,z=h,t)=0. \end{cases} \tag{1}$$

Potential distribution $V_e(x,y,t)$ is created by the biased probe of force microscope. The probe is assumed to be in perfect electric contact with the sample surface. Electrostatic potential $\varphi(\mathbf{r},t)$ includes the effects of depolarization field created by polarization bound charges; ε_0 is the dielectric constant and h is the film thickness. The perfect screening of depolarization field outside the sample is realized by the ambient charges, as shown in Fig. 1(a).

The polarization $P_3(\mathbf{r},t)$ in uniaxial ferroelectrics is directed along the polar axis z. The sample is dielectrically isotropic in transverse directions, i.e., permittivities $\varepsilon_{11}=\varepsilon_{22}$. The dependence of in-plane polarization components on electric field is linearized as $P_{1,2}\approx-\varepsilon_0(\varepsilon_{11}-1)\partial\varphi(\mathbf{r})/\partial x_{1,2}$. We can rewrite the problem (1) for quasistatic electrostatic potential as

$$\begin{cases} \varepsilon_{33}^b\dfrac{\partial^2\varphi}{\partial z^2}+\varepsilon_{11}\left(\dfrac{\partial^2\varphi}{\partial x^2}+\dfrac{\partial^2\varphi}{\partial y^2}\right)=\dfrac{1}{\varepsilon_0}\dfrac{\partial P_3}{\partial z}, \\ \varphi(x,y,z=0)=V_e(x,y,t), \qquad \varphi(x,y,z=h)=0. \end{cases} \tag{2}$$

Here we introduced dielectric permittivity of background[18] or reference state[19] as ε_{33}^b. Typically $\varepsilon_{33}^b\leq 10$. The background contribution origin can be related to the contribution of dielectric polarizability from the nonferroelectric lattice modes of the crystal.[18]

The corresponding Fourier-Laplace representation on transverse coordinates $\{x,y\}$ and time t of electric-field normal component $\tilde{E}_3(\mathbf{k},z,f)=-\partial\tilde{\varphi}/\partial z$ is the sum of external (e) and depolarization (d) fields,

$$\tilde{E}_3(\mathbf{k},z,f)=\tilde{E}_3^e(V_e,\mathbf{k},z,f)+\tilde{E}_3^d(P_3,\mathbf{k},z,f), \tag{3a}$$

$$\tilde{E}_3^e(\mathbf{k},z,f)=\tilde{V}_e(\mathbf{k},f)\frac{\cosh[k(h-z)/\gamma_b]}{\sinh(kh/\gamma_b)}\frac{k}{\gamma_b}, \tag{3b}$$

$$\begin{aligned}\tilde{E}_3^d(P_3,\mathbf{k},z,f) &= \left\{\int_0^z dz'\frac{\tilde{P}_3(\mathbf{k},z',f)}{\varepsilon_0\varepsilon_{33}^b}\cosh(kz'/\gamma_b)\frac{\cosh[k(h-z)/\gamma_b]}{\sinh(kh/\gamma_b)}\frac{k}{\gamma_b}\right. \\ &+\int_z^h dz'\frac{\tilde{P}_3(\mathbf{k},z',f)}{\varepsilon_0\varepsilon_{33}^b}\cosh[k(h-z')/\gamma_b]\frac{\cosh(kz/\gamma_b)}{\sinh(kh/\gamma_b)}\frac{k}{\gamma_b} \\ &\left.-\frac{\tilde{P}_3(\mathbf{k},z,f)}{\varepsilon_0\varepsilon_{33}^b}\right\}.\end{aligned} \tag{3c}$$

Here $\gamma_b=\sqrt{\varepsilon_{33}^b/\varepsilon_{11}}$ is the "bare" dielectric anisotropy factor, $\mathbf{k}=\{k_1,k_2\}$ is a spatial wave vector, $k=\sqrt{k_1^2+k_2^2}$ its absolute value, and f is temporal frequency of Laplace transformation. The corresponding Fourier-Laplace image of polarization is $\tilde{P}_3(\mathbf{k},z,f)=(1/2\pi)\int_0^\infty dt\int_{-\infty}^\infty dx\int_{-\infty}^\infty dy\,\exp(ik_1x+ik_2y-ft)P_3(x,y,z,t)$. $\tilde{V}_e(\mathbf{k},f)$ is the Fourier-Laplace image of electric-field potential at the sample surface. For a transversally homogeneous media, $\varepsilon_{33}^b=1$ and the static case Eq. (3c) reduces to the expression for depolarization field obtained by Kretschmer and Binder.[20]

In the framework of GLD phenomenology, the spatial-temporal evolution of the polarization component P_3 of the second-order ferroelectric is described by the Landau-Khalatnikov equation

$$-\tau\frac{d}{dt}P_3=\alpha P_3+\beta P_3^3-\xi\frac{\partial^2P_3}{\partial z^2}-\eta\left(\frac{\partial^2P_3}{\partial x^2}+\frac{\partial^2P_3}{\partial y^2}\right)-E_3. \tag{4}$$

The gradient terms are $\xi>0$ and $\eta>0$; the expansion coefficients are $\alpha<0$ in ferroelectric phase, $\beta<0$ for the first-order phase transitions, and $\beta>0$ for the second-order ones; and τ is the Khalatnikov coefficient (relaxation time). In the absence of (microscopic) pinning centers or for weak pinning of viscous friction type, the domain-wall equilibrium profile can be found as stationary solution of Eq. (4). Rigorously, coefficient α should be taken as renormalized by the elastic stress as $\alpha-2Q_{ij33}\sigma_{ij}$.[21,22] Hereinafter we neglect the striction effects, which are relatively small for $LiTaO_3$ and $LiNbO_3$.[23]

The initial and boundary conditions for polarization in Eq. (4) are

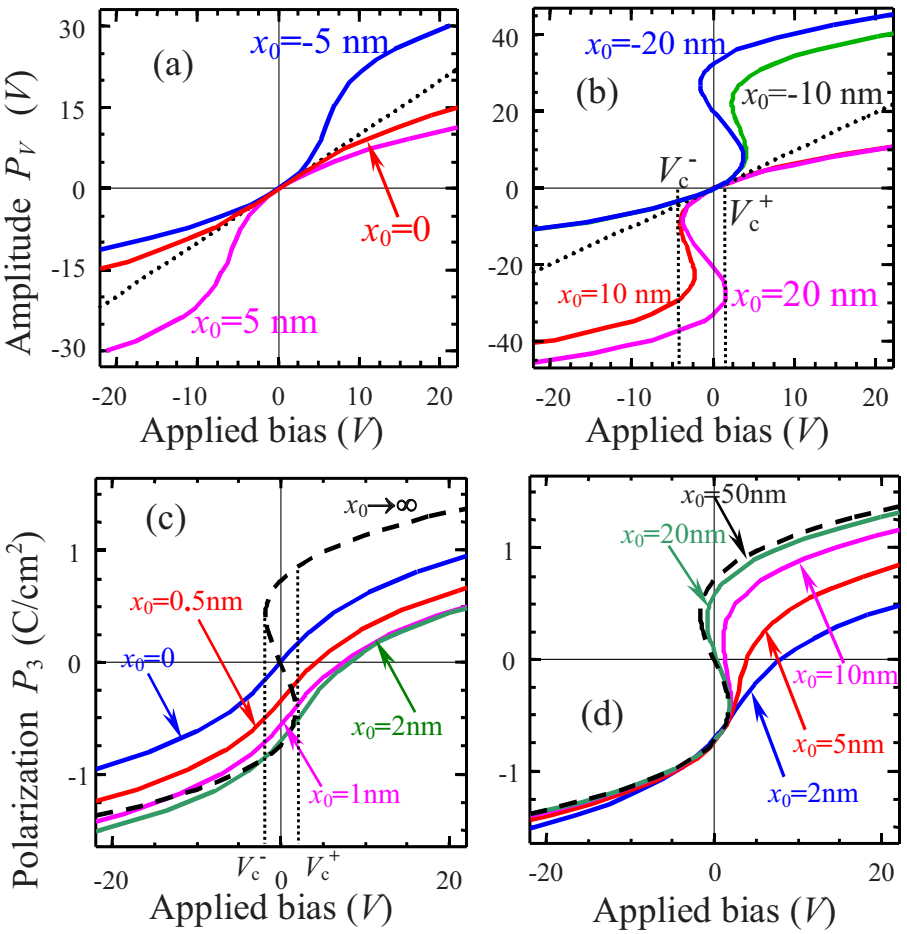

FIG. 2. (Color online) (a) and (b) Bias dependence of P_V on applied bias V for different domain-wall initial position x_0 (labels near the curves in nanometer). Effective distance d=5 nm and material parameters for $LiNbO_3$ are ε_{11}=84, $\alpha=-2\times10^9$, $\eta=10^{-9}$ in SI units (i.e., $L_\perp$=0.5 nm), and P_S=0.75 C/m^2. Dotted curves is linear approximation $P_V=V$ that works satisfactorily up to 5 V for the chosen material parameters. (c) and (d) Polarization below the probe apex $P_3(0)$ for different x_0 values (labels near the curves in nanometer).

$$P_3(\mathbf{r},t\le 0)=P_0(\mathbf{r}),\qquad \left(P_3-\lambda_1\frac{\partial P_3}{\partial z}\right)\bigg|_{z=0}=0,$$
$$\left(P_3+\lambda_2\frac{\partial P_3}{\partial z}\right)\bigg|_{z=h}=0. \tag{5}$$

Here $P_0(\mathbf{r})$ is the initial profile of domain wall that satisfies Eq. (4) for zero external field. The extrapolation lengths $\lambda_{1,2}$ may be different for z=0 and h, reflecting the difference in boundary conditions (e.g., free surface and ferroelectric-electrode interface for thin film, or dissimilar electrodes for capacitor structure or thin dielectric layer on the surface). Reported extrapolation length values are 0.5–50 nm.[24]

Equations (4) and (5) are the closed-form three-dimensional-boundary problem for the determination of the equilibrium domain-wall profile. The free-energy excess related to the polarization redistribution caused by the external electric field E_3^e can be defined as the energy difference ΔG between the initial-state free energy $G(P_0,E_3^e)$ and the final-state free energy $G(P_3,E_3^e)$ with equilibrium polarization distribution $P_3(x,y,z)$ found from Eq. (4),

$$\Delta G(P_3,E_3^e)=G(P_0,E_3^e)-G(P_3,E_3^e), \tag{6}$$

$$G(P,E_3^e)=\int_{-\infty}^{\infty}dx\int_{-\infty}^{\infty}dy\left\{\int_0^h dz\left[\frac{\alpha}{2}P^2+\frac{\beta}{4}P^4+\frac{\xi}{2}\left(\frac{\partial P}{\partial z}\right)^2+\frac{\eta}{2}(\nabla_\perp P)^2-P\left(E_3^e+\frac{E_3^d}{2}\right)\right]+\frac{\xi}{2\lambda_1}P^2(z=0)+\frac{\xi}{2\lambda_2}P^2(z=h)\right\}. \tag{7}$$

In the continuous media approximation, the stable domain-wall boundary $x_{DW}(y,z)$ can be defined from the condition $P_3(x_{DW},y,z,t\gg\tau)=0$.

For the global excitation of ferroelectric sample with homogeneous external field E_0^e, the energetic barrier ΔG_a required to move the domain-wall boundary by overcoming the effect of the lattice discreteness (the simplest pinning model) can be estimated as the difference between the initial-state free energy $G(P_0,E_0^e)$ and the equilibrium state $G(P_3,E_0^e)$ with the domain boundary local deviation from initial profile equal to lattice constant a.[1] However the simple criteria should be modified for the considered case of probe-induced domain-wall bending, since probe-induced domain

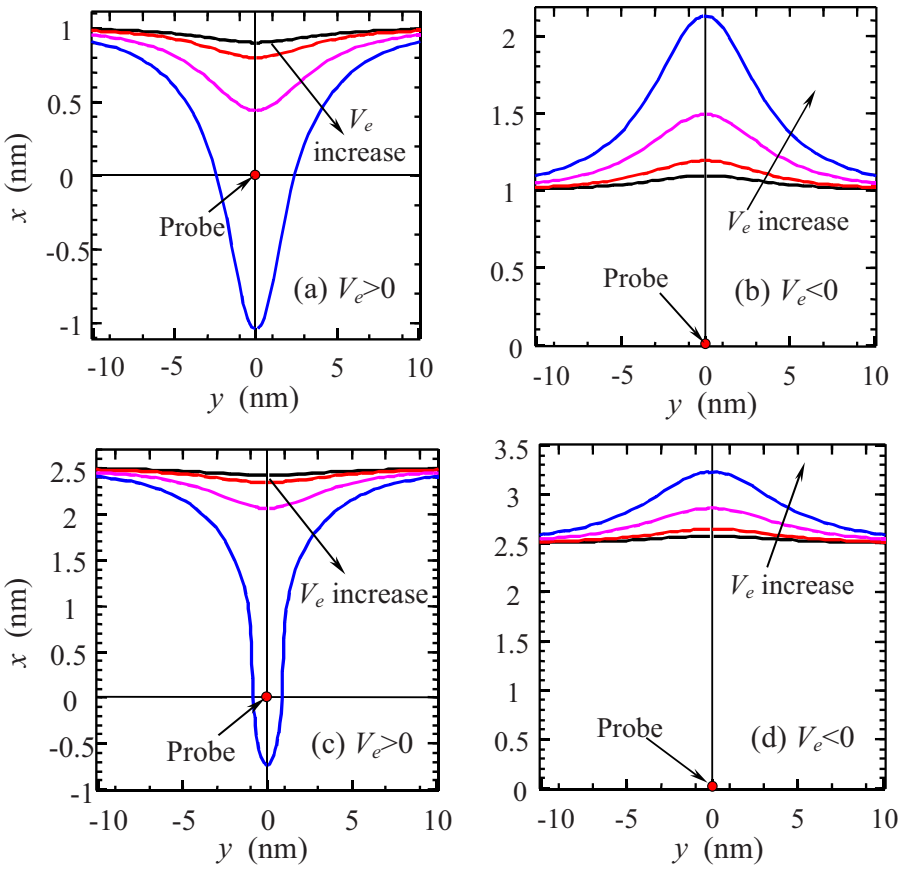

FIG. 3. (Color online) Equilibrium surface profile of domain wall affected by biased probe. Material parameters for $LiNbO_3$ are $\varepsilon_{11}=84$, $\alpha=-2\times10^9$, $\eta=10^{-9}$ in SI units (i.e., $L_\perp=0.5$ nm), and $P_S=0.75$ C/m^2. Effective distance $d=5$ nm and initial domain-wall position $x_0=1$ nm for plots (a) and (b), while $x_0=2.5$ nm for plots (c) and (d). Different curves correspond to different voltages applied to the probe. Positive $V=1,2,5,10$ V for plots (a) and (c) and negative $V=-1,-2,-5,-10$ V for plots (b) and (d).

nucleation far from the wall could appear. The behavior is analyzed in more detail in Sec. IV.

For the global excitation of ferroelectric sample with relatively small homogeneous external field E_3^e, the dependence of domain-wall velocity $\mathbf{v}$ on the electric field usually has exponential form $\mathbf{v}\sim\exp(-E_a/E_0^e)$ in the regime of thermal activation mechanism of domain-wall movement.[1] In the Miller-Weinreich model, the critical nucleus size determines the activation energy and thus activation field E_a.

To determine the velocity $\mathbf{v}(x,y,z,t)$ of the domain-wall movement far from the activated regime (i.e., in the very large field limit) one can use the substitution $dP_3(\mathbf{r}-\mathbf{v}t)/dt=-\mathbf{v}\nabla Pt$ and corresponding equation for the order parameter.[25] Keeping in mind that the right-hand side of Eq. (4) is the free energy (6) variation derivative $\partial G(P_3)/\partial P_3$, one obtains

$$v_i(x,y,z,t)=\frac{\partial G(P_3)/\partial P_3}{\tau(\partial P_3/\partial x_i)},\quad (i=1,2,3). \tag{8}$$

It is clear that the velocity tends to become zero in thermodynamic equilibrium $\partial G(P_3)/\partial P_3=0$, as anticipated. Far from the equilibrium, the variation derivative $\partial G(P_3)/\partial P_3$ can be regarded as generalized pressure similarly to the pressure introduced in the rigid model for domain nucleation as considered by Molotskii and Shvebelman.[26] Below, we proceed with the analysis of the domain-wall geometry and thermodynamics as a key component in the analysis of wall dynamics. The effects of lattice and defect pinning on wall dynamics will be analyzed elsewhere.

III. THERMODYNAMICS OF DOMAIN-WALL INTERACTION WITH BIASED PROBE

A. Direct variational method

Hereinafter, we consider semi-infinite second-order ferroelectrics with large extrapolation length $\lambda_1\gg\sqrt{\xi}$. Infinite extrapolation length $\lambda_1\to\infty$ corresponds to the situation of perfect atomic surface structure without defects or damaged layer. Corresponding surface energy proportional to $(\xi/2\lambda_1)P_3^2(z=0)$ is negligibly small, and hence the domain-wall energy is determined only by correlation term $(\xi/2)(\partial P_3/\partial z)^2+(\eta/2)(\nabla_\perp P_3)^2$. Mathematical details of calculations for much more cumbersome case of finite extrapolation length $\lambda_{1,2}<\infty$ and sample thickness $h<\infty$ are available in Appendices A and B of Ref. 27.

Potential distribution produced by the SPM probe on the surface is approximated as $V_e(x,y,t\geq0)\approx Vd/\sqrt{x^2+y^2+d^2}$, where V is the applied bias and d is the effective distance

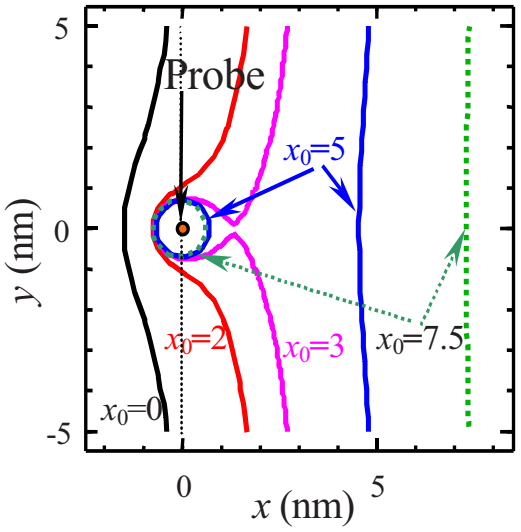

FIG. 4. (Color online) Equilibrium surface profile of domain-wall boundary affected by biased probe (for $x_0=0,2,3$ nm) and probe-induced domain formation (for $x_0=5,7.5$ nm). Effective distance $d=5$ nm, applied bias $V=5$ V, and $LiNbO_3$ material parameters are listed in Fig. 3.

determined by the probe geometry.[13,14] The potential is normalized assuming the condition of perfect electrical contact with the surface, $V_e(0,0,t\geq 0)\approx V$. The corresponding Fourier-Laplace image for a point-charge approximation of a probe is

$$\tilde{V}_e(\mathbf{k},f)=V\frac{\tilde{w}(\mathbf{k})}{f},\quad \tilde{w}(\mathbf{k})=\frac{d}{k}\exp(-kd). \tag{9}$$

In the case of local point-charge model, the probe is represented by a single charge $Q=2\pi\varepsilon_0\varepsilon_e R_0 V(\kappa+\varepsilon_e)/\kappa$ located at $d=\varepsilon_e R_0/\kappa$ for a spherical tip apex with curvature R_0 [$\kappa\approx\sqrt{(\varepsilon_{33}^b-1/2\varepsilon_0\alpha)\varepsilon_{11}}$ is the effective dielectric constant determined by the "full" dielectric permittivity in z-direction, ε_e is ambient dielectric constant], or $d=2R_0/\pi$ for a flattened tip represented by a disk of radius R_0 in contact with the sample surface.[13,14]

Using the perturbation theory, we search for the solution of Eq. (4) in the form

$$P_3(\mathbf{r},t)=P_0(x)+p(\mathbf{r},t). \tag{10a}$$

Polarization distribution $P_0(x)$ satisfies Eq. (4) at zero external bias $V_e=0$. Equation (4) reduces to $\alpha P_0(x)+\beta P_0(x)^3-[\eta(\partial^2 P_0(x)/\partial x^2)]=0$. The solution for the initial flat domain-wall profile positioned at $x=x_0$ is

$$P_0(x)=P_S\tanh[(x-x_0)/2L_\perp], \tag{10b}$$

where the correlation length is $L_\perp=\sqrt{-\eta/2\alpha}$ and the spontaneous polarization is $P_S^2=-\alpha/\beta$.

Since the distribution $P_0(x)$ does not cause depolarization field, the operator $E_3^d[P_0(x)+p(\mathbf{r},t)]=E_3^d[p(\mathbf{r},t)]\neq 0$, i.e., depolarization effect is determined by the wall curvature. Hence, the Eq. (4) with substitutions (10a) and (10b) acquires the form

$$\tau\frac{dp}{dt}-\{2\alpha+3\beta[P_S^2-P_0(x)^2]\}p+3\beta P_0(x)p^2+\beta p^3-\xi\frac{\partial^2 p}{\partial z^2}-\eta\left(\frac{\partial^2 p}{\partial x^2}+\frac{\partial^2 p}{\partial y^2}\right)=E_3[V_e,p]. \tag{11a}$$

Initial and boundary conditions for perturbation $p(x,y,z,t)$ are

$$p(\mathbf{r},t\leq 0)=0,\qquad \left.\frac{\partial p}{\partial z}\right|_{z=0}=0. \tag{11b}$$

In continuous media approximation adopted here, in the immediate vicinity of domain-wall polarization tends to become zero and thus Eq. (11a) could be linearized with respect to deviation p from initial profile P_0. Using the method of slow-varying amplitudes[28] for the linearized Eq. (11a) with x-dependent coefficient, we derived the linearized solution of Eqs. (11a) and (11b) as

$$\tilde{p}(\mathbf{k},z,f)\approx\varepsilon_{33}^b\varepsilon_0 V\frac{\tilde{w}(k)}{f}\frac{(k^2/\gamma_b^2-s_1^2)(k^2/\gamma_b^2-s_2^2)}{s_1 s_2(s_1^2-s_2^2)}[s_2\exp(-s_1 z)-s_1\exp(-s_2 z)]. \tag{12}$$

Eigenvalues $s_{1,2}(k,f)$ are positive roots of biquadratic equation $(s^2-k^2/\gamma_b^2)(-2\alpha_S+\eta k^2-\xi s^2)=-s^2/(\varepsilon_0\varepsilon_{33}^b)$, namely,

$$s_{1,2}^2=\frac{1+[k^2(\xi/\gamma_b^2+\eta)-2\alpha_S]\varepsilon_0\varepsilon_{33}^b}{2\varepsilon_0\varepsilon_{33}^b\xi}\pm\frac{1}{2\varepsilon_0\varepsilon_{33}^b\xi}\sqrt{\{1+[k^2(\xi/\gamma_b^2+\eta)-2\alpha_S]\varepsilon_0\varepsilon_{33}^b\}^2-4(\varepsilon_{33}^b\varepsilon_0)^2\xi(k^2\eta-2\alpha_S)k^2/\gamma_b^2}. \tag{13}$$

Note, that depolarization field (terms proportional to ε_0) and correlation effects (terms proportional to ξ and η) determine the spectrum $s_{1,2}(k,f)$. In Appendix A of Ref. 27, we have shown that the effective coefficient α_S is renormalized by finite correlation length and lattice relaxation as

$$\alpha_S(x_0,L_\perp,f)=\alpha\left\{1-\frac{6L_\perp(L_\perp+d)}{\pi[(L_\perp+d)^2+x_0^2]}\right\}-\frac{\pi f}{2}. \tag{14}$$

Solution (12) is valid at small biases V, for which the amplitude p remained small in comparison with P_S.

To obtain the domain-wall profile at arbitrary bias we used direct variational method.[29,30] In this method, **k**-dependent (i.e., coordinate-dependent) part of linearized solution (12) was used as the trial function in the free-energy functional $\Delta G(P_3, E_3^e)$ given by Eqs. (6) and (7), while the amplitude was treated as a variational parameter P_V, whose dimensionality is volts. The consequence of this analysis is that P_V is a single parameter determining wall geometry and contributing to free energy. Hence, system thermodynamics is now described by a single scalar quantity rather than wall coordinates (much like scalar order parameter in GLD).

Direct integration of $\Delta G(P_3, E_3^e)$ along with Eqs. (9), (10a), (10b), (11a), (11b), and (12) allows us to determine the amplitude P_V as the solution of nonlinear algebraic equation (see Appendix C of Ref. 27 for mathematical details). Allowing for the radial symmetry of normalized probe potential $\tilde{w}(k)$, after elementary algebraic transformations, we obtained the dependence of the *equilibrium solution* and the free-energy functional on the applied bias V and other parameters in the form

$$P_3(\mathbf{r}) \approx P_0(x) - P_V \int_0^\infty \frac{k^2}{\gamma_b} dk J_0(k\sqrt{x^2+y^2})\tilde{w}(k) \times \frac{[s_2 \exp(-s_1 z) - s_1 \exp(-s_2 z)]}{\sqrt{\xi(\eta k^2 - 2\alpha_S)}(s_1^2 - s_2^2)}, \tag{15a}$$

$$\Delta G(P_V) \approx \pi d \sqrt{\frac{\varepsilon_0 \varepsilon_{11}}{-2\alpha_S}} \left(-P_V V + \frac{P_V^2}{2} + \frac{w_3}{3} P_V^3 + \frac{w_4}{4} P_V^4 \right), \tag{15b}$$

$$P_V + w_3 P_V^2 + w_4 P_V^3 = V, \tag{15c}$$

where J_0 is Bessel function of zero order and the roots $s_{1,2}$ and coefficient α_S are given by Eqs. (13) and (14) under the condition $f=0$ used hereinafter. Parameters

$$w_3(x_0) = \frac{-3\beta P_S x_0}{\sqrt{(L_\perp + d)^2 + x_0^2}} \frac{\sqrt{-2\alpha_S \varepsilon_{11} \varepsilon_0}}{4\alpha_S^2 (L_\perp + d)}, \quad w_4 = \frac{\beta \varepsilon_{11} \varepsilon_0}{4\alpha_S^2 (L_\perp + d)^2} \tag{16}$$

are introduced.

Note, that Eq. (15a) is ε_{33}^b dependent via $\gamma_b = \sqrt{\varepsilon_{33}^b / \varepsilon_{11}}$ and Eq. (13), while bare dielectric permittivity ε_{33}^b canceled in Eqs. (15b) and (16) since they contain only the product $\varepsilon_{11}\varepsilon_0$.

Both surface and depth profiles of equilibrium polarization distribution perturbed by the biased probe can be calculated from Eq. (15a), where the bias dependence $P_V(V)$ is given by nonlinear Eq. (15c).

The bias dependence of the amplitude $P_V(V)$ given by cubic Eq. (15c) is shown in Figs. 2(a) and 2(b) for different x_0 values and $LiNbO_3$ material parameters. Note, that Eq. (15c) reproduces the main features of the ferroelectric hysteresis far from the domain wall (i.e., bistability between the state with single domain wall and the state with nascent domain is possible at $|x_0| \gtrsim d$) as shown in Fig. 2(b). This is a direct consequence of GLD model (as opposed to rigid ferroelectric model) adopted here.

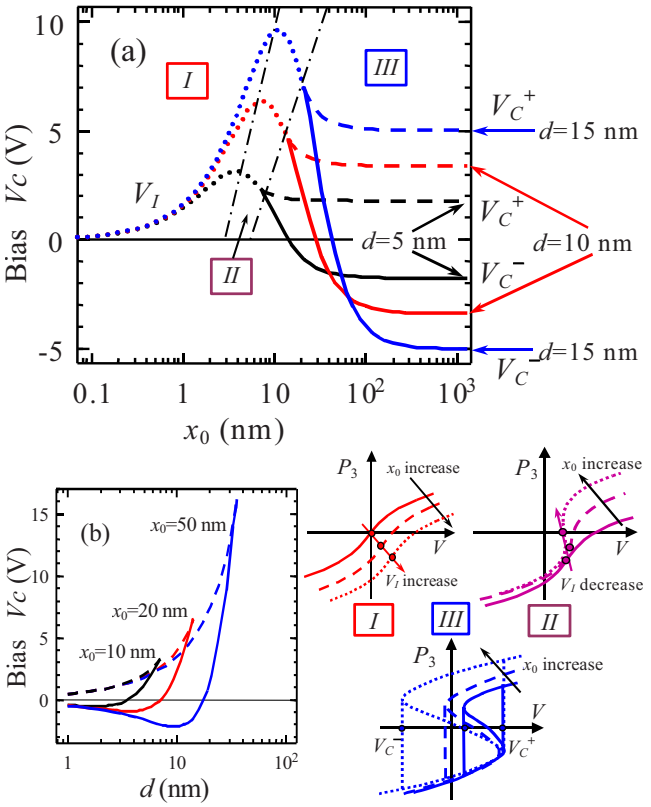

FIG. 5. (Color online) (a) Dependence of probe-induced domain formation coercive biases V_c^+ (dashed curves) and V_c^- (solid curves) vs the distance x_0 between the domain wall and the probe apex. Separation d between the effective charge modeling the probe field and sample surface is fixed as 5, 10 and 15 nm (right labels with arrows). In the region where hysteresis is absent, dotted curves represent the bias V_I at inflection point of polarization dependence on bias. Polarization P_3 bias dependence in the regions I (no hysteresis loop, inflection point bias V_I increases with distance x_0 increase as shown by arrow cross section with solid, dashed, and dotted curves), II (no hysteresis loop, inflection point bias V_I slightly decreases with distance x_0 increase as shown by arrow cross section with solid, dashed, and dotted curves), and III (hysteresis loop appears and becomes symmetric with distance x_0 increase as shown by solid, dashed, and dotted curves) is schematically shown below at insets I–III. (b) Coercive biases V_c^+ (dashed curves) and V_c^- (solid curves) dependence vs the effective distance d for the wall-probe distance x_0 fixed as 10, 20 and 50 nm (labels near the curves). Parameters of $LiNbO_3$ are the same as in Fig. 3.

Thermodynamic coercive bias $V_c^\pm$ can then be found from the condition $dV/dP_V = 0$, namely,

$$V_c^\pm = \frac{w_3(2w_3^2 - 9w_4) \pm 2(w_3^2 - 3w_4)^{3/2}}{27w_4^2}. \tag{17}$$

Corresponding hysteresis loop halfwidth $\Delta V_c = (V_c^+ - V_c^-)/2$ and imprint bias $V_I = (V_c^+ + V_c^-)/2$ are

$$\Delta V_c = \frac{2(w_3^2 - 3w_4)^{3/2}}{27w_4^2}, \tag{18a}$$

$$V_I = \frac{w_3(2w_3^2 - 9w_4)}{27w_4^2}. \tag{18b}$$

It is easy to show that ΔV_c is defined only for the case of $x_0^2 \geq 2(L_\perp + d)^2$. Only in this region the bistability is possible. The coercive biases properties will be considered in details in Sec. IV. In Sec. III B we show that the hysteresis corresponds to the stable domain formation below the tip apex. At zero bias, the bistable nonzero solutions $P_V(V=0) = (-w_3 \pm \sqrt{w_3^2 - 4w_4})/2w_4$ appear under the condition $w_3^2 \geq 4w_4$. The latter inequality is equivalent to condition $x_0^2 \geq 8(L_\perp + d)^2$ (see Appendix C for details in Ref. 27).

B. Equilibrium surface profile of domain wall perturbed by the biased probe

At the sample surface $z=0$, stationary solution, given by Eq. (15a) at $f=0$, can be simplified as

$$P_3(x,y,0) = P_0(x) + \int_0^\infty \frac{dkk^2\sqrt{\varepsilon_{11}\varepsilon_0}J_0(k\sqrt{x^2+y^2})(\eta k^2 - 2\alpha_S)^{-1/2}\tilde{w}(k)P_V(V)}{\sqrt{1 + \varepsilon_0[k^2(\varepsilon_{11}\xi + \eta\varepsilon_{33}^b) - 2\varepsilon_{33}^b\alpha_S] + 2\varepsilon_0 k\sqrt{\xi\varepsilon_{11}\varepsilon_{33}^b(\eta k^2 - 2\alpha_S)}}}. \tag{19}$$

For a point-charge approximation of a probe, $\tilde{w}(k) = d\exp(-kd)/k$ in accordance with Eq. (9). For typical ferroelectric material parameters and $\varepsilon_{33}^b \leq 10$, the inequality $2\varepsilon_0\varepsilon_{33}^b|\alpha| \ll 1$ is valid, and so the integral in Eq. (19) reduces to the approximate explicit form (see Appendix D for details of Ref. 27)

$$P_3(x,y,0) \approx P_0(x) + \frac{\sqrt{\varepsilon_{11}\varepsilon_0/(-2\alpha_S)}d^2 \cdot P_V(V)}{[d\sqrt{\eta/(-2\alpha_S)} + d^2 + x^2 + y^2]\sqrt{d^2 + x^2 + y^2}}. \tag{20a}$$

In particular, polarization below the probe apex has the form

$$P_3(\mathbf{r}=0) \approx -P_S \tanh\left(\frac{x_0}{2L_\perp}\right) + \sqrt{\frac{\varepsilon_{11}\varepsilon_0}{-2\alpha_S}}\frac{P_V(V)}{[\sqrt{\eta/(-2\alpha_S)} + d]}. \tag{20b}$$

The bias dependence of $P_3(\mathbf{r}=0)$ is illustrated in Figs. 2(c) and 2(d) for different x_0 values.

Under the absence of pinning centers, thermodynamically equilibrium domain-wall boundary $x_{\mathrm{DW}}(y)$ can be determined from the condition $P_3(x_{\mathrm{DW}},y,0)=0$. Using expression (10b) for $P_0(x_{\mathrm{DW}})$ in Eq. (20), we obtained the parametric dependences

$$x_{\mathrm{DW}}(\rho) = x_0 + 2L_\perp \operatorname{arctanh}\left\{\frac{-\sqrt{\varepsilon_{11}\varepsilon_0/(-2\alpha_S)}d^2 \cdot P_V/P_S}{[d^2 + \rho^2 + \sqrt{\eta/(-2\alpha_S)}d]\sqrt{d^2+\rho^2}}\right\}, \tag{21a}$$

$$y_{\mathrm{DW}}^2(\rho) = \rho^2 - x_{\mathrm{DW}}^2(\rho), \tag{21b}$$

valid near the wall ($|x_0| \ll d$). Parameter ρ is the radial coordinate. Far from the wall ($|x_0| > L_\perp + d$), the equilibrium domain appears at biases larger the coercive. The corresponding radius $\rho(V)$ can be determined from the cubic equation

$$\left(d^2 + \rho^2 + d\sqrt{\frac{\eta}{-2\alpha_S}}\right)\sqrt{d^2+\rho^2} = d^2\sqrt{\frac{\varepsilon_{11}\varepsilon_0}{-2\alpha_S}}\frac{P_V(V)}{P_S\tanh(x_0/2L_\perp)}. \tag{22}$$

Equilibrium surface profile of domain wall affected by biased probe is shown in Fig. 3 for $LiNbO_3$ material parameters. For a chosen polarization distribution, the wall attraction to the probe corresponds to positive biases [see Figs. 3(a) and 3(c)], while the domain-wall repulsion from the probe takes place at negative biases [see Figs. 3(b) and 3(d)]. For chosen material constants and probe parameter $d=5$ nm, characteristic depth of domain-wall bending is close to d, as anticipated from Eq. (15a). Note that domain-wall boundary bending by biased probe is observed at distances $|x_0| < d$ (see Fig. 4 for $x_0 = 0, 2, 3$ nm), while the probe-induced domain formation appears at $|x_0| > d$ (see Fig. 4 for $x_0 = 5, 7.5$ nm).

IV. DISCUSSION

Dependence of thermodynamic coercive bias for probe-induced domain formation $V_c^\pm$ calculated from Eq. (17) on the distances x_0 and d is shown in Figs. 5(a) and 5(b) by dashed and solid curves, correspondingly. The presence of $V_c^\pm$ indicates the ferroelectric hysteresis appeared in the region $x_0^2 > 2(L_\perp + d)^2$. The asymmetry of $V_c^\pm$ corresponds to the domain nucleation and bending toward or away from the tip [compare dashed and solid curves in Figs. 5(a)].

Hysteresis bias changes near the domain wall is due to the fact that the wall can bend toward or away from the tip and its depolarization electric field facilitates or impedes the tip-induced domain nucleation. As shown in Fig. 5(b), V_c^+ curves are monotonic since the tip and depolarization field add together (see dashed curves); V_c^- curves have minimum since the tip and depolarization field are opposite (see solid curves).

In the region $|x_0| < \sqrt{2}(L_\perp + d)$, hysteresis is absent. Only the domain-wall bending in different directions depending on

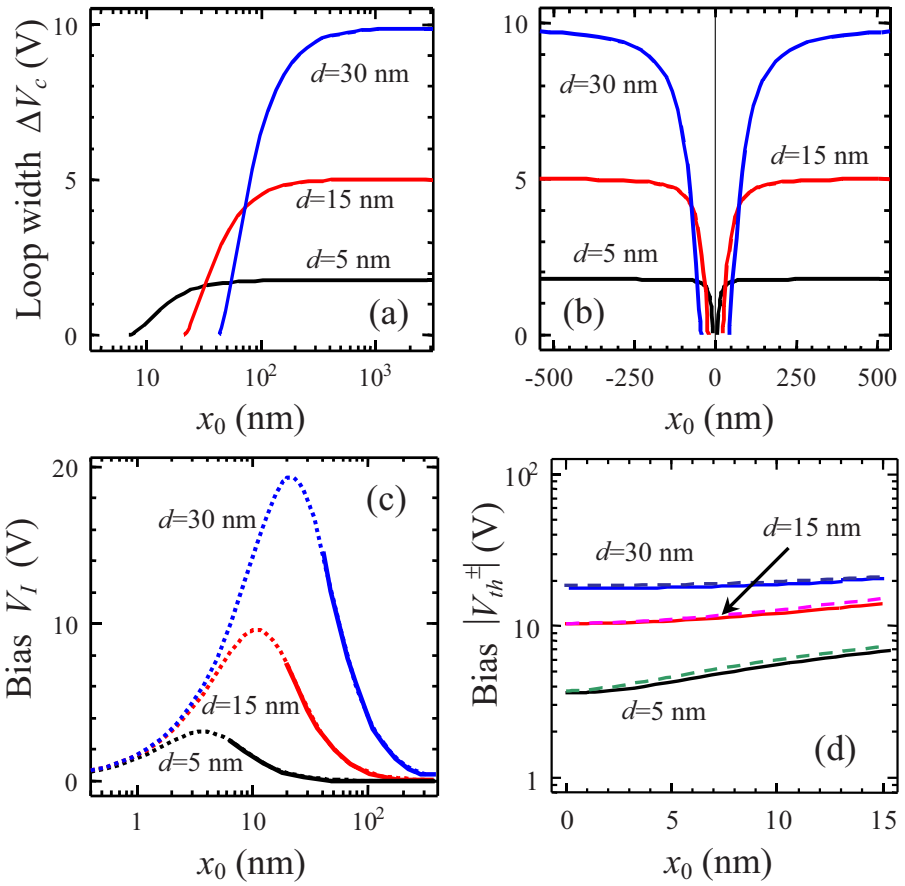

FIG. 6. (Color online) Dependence of probe-induced domain formation hysteresis loop width $\Delta V_c=(V_c^+-V_c^-)/2$ in linear-log (a) and linear (b) scales as the function of the distance x_0 between the domain wall and the probe apex for different effective charge-surface distances d=5, 10 and 30 nm (labels near the curves). (c) The inflection point bias V_I (dotted curves) and hysteresis loop imprint bias $V_I=(V_c^+ + V_c^-)/2$ (solid curves) vs the distance x_0 for the same d=5, 10 and 30 nm (labels near the curves). (d) Absolute values of threshold biases V_{th}^+ (solid curves) and V_{th}^- (dashed curves) required to move the domain-wall boundary by overcoming the effect of the lattice-constant discreteness as the function of the distance x_0 for d=5, 10 and 30 nm (labels near the curves). Parameters of $LiNbO_3$ are the same as in Fig. 3.

the bias sign takes place. The dotted curves correspond to the bias V_I given by Eq. (18b), i.e., the inflection point of polarization dependence on bias where the second derivative d^2P_V/dV^2 is zero. It can be easily shown that this quantity corresponds to the loop imprint $V_I=(V_c^+ + V_c^-)/2$ in the hysteresis region. Appearance of maximum on V_I curves can be attributed to the linear and nonlinear contributions w_3 and w_4 of different signs, while both contributions are monotonic functions of x_0 [see Eq. (16) and insets I–III]. Physically, the imprint bias originates from nonzero depolarization field (3c) induced by the curved domain wall and nonlinear long-range interactions $\sim P^4$ asymmetry near the wall. Note that depolarization field is zero for the initial wall profile $P_0(x)$. From the symmetry considerations, depolarization field and interaction energy are zero when the tip is exactly at the wall, i.e., x_0=0. The domain-wall bending results in the depolarization field that facilitates domain nucleation in the proximity of the bend, thus reducing local nucleation bias. The interaction energy asymmetry vanishes far from the wall when the nucleating domain shape becomes axially symmetric. Basically, the peak of the imprint represents, for a tip effective parameter d, the intermediate region where the wall influence is seen, but also independent nucleation begins to occur (e.g., as shown in Fig. 4 for x_0=3 nm).

The dependence of hysteresis loop halfwidth $\Delta V_c=(V_c^+ - V_c^-)/2$ given by Eq. (18a) and imprint bias V_I given by Eq. (18b) via the domain-wall position x_0 is shown in Fig. 6 for different d values.

As it was mentioned in Sec. II, the equilibrium domain-wall bending could start at an infinitely small probe bias only in the continuous medium approximation (no lattice or defect pinning). Let us postulate that the threshold (or critical) bias V_{th} is required to move the domain-wall boundary by overcoming the effect of the lattice-constant a discreteness. For the considered case of one-dimensional-initial profile $P_0(x)$, maximal local deviation from the initial profile $x_{\text{DW}}=x_0$ appears at the sample surface [see Fig. 1(b)]. In the activationless region $|x_0|<\sqrt{2}(L_\perp+d)$, absolute values of positive and negative threshold biases $V_{\text{th}}^{\pm}$ should be found numerically from the condition $\max\{|x_0-x_{\text{DW}}(y=0,z=0)|\}=a$ allowing for Eqs. (20a) and (15c). Absolute values of positive and negative threshold bias $V_{\text{th}}^{\pm}$ via x_0 are shown in Fig. 6(d) by solid and dashed curves respectively. In the case $|x_0| \ll 2(L_\perp+d)$, amplitude $P_V \approx V$ is with high accuracy, allow-

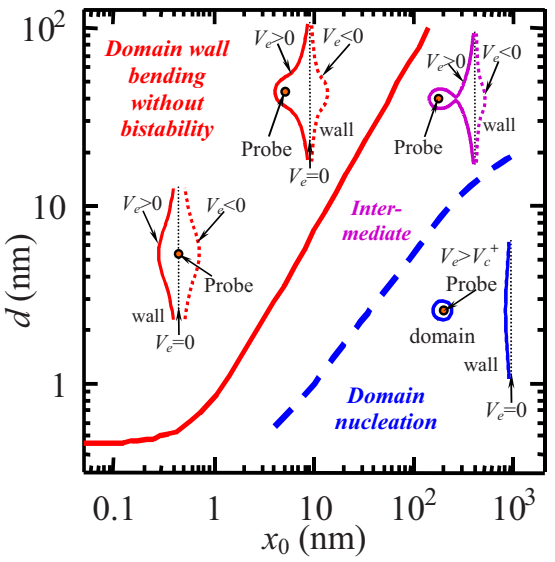

FIG. 7. (Color online) Phase diagram in coordinates $\{x_0, d\}$. Boundaries between the regions of different bias dependence of P_3. Activationless domain-wall bending, domain nucleation far from the wall (hysteresis), and intermediate regimes are shown schematically. Material parameters of $LiNbO_3$ are the same as in Fig. 5.

ing for the small value of lattice constant $a \sim 0.5$ nm. So, using Eq. (21a), one leads to the expressions for negative and positive threshold biases (see Appendix D of Ref. 27 for mathematical details)

$$V_{\text{th}}^{\pm} = \pm \sqrt{\frac{-2\alpha_S}{\varepsilon_{11}\varepsilon_0}} \tanh\left(\frac{a}{2L_\perp}\right) \frac{P_S}{d^2}[d^2 + (x_0 \pm a)^2 + L_\perp d]\sqrt{d^2 + (x_0 \pm a)^2}. \quad (23)$$

For infinitely thin domain wall $L_\perp \to 0$, and hence Eq. (23) leads to the expression $V_{\text{th}}^{\pm} \to \pm\sqrt{-2\alpha/(\varepsilon_{11}\varepsilon_0)} P_S[d^2 + (x_0 \pm a)^2]^{3/2}/d^2$.

The phase diagram in coordinates $\{x_0, d\}$ that contains domain-wall bending regime (no hysteresis, $V_c^{\pm} = 0$) to the domain nucleation far from the wall (almost symmetric hysteresis loop with $V_c^+ \approx -V_c^-$) and intermediate regime (asymmetric hysteresis with $V_c^+ \neq -V_c^-$) is shown in Fig. 7.

For the second-order ferroelectrics considered here, nonzero energetic barrier for polarization reorientation existing in the range of hysteresis, namely, at distances $|x_0| > \sqrt{2}(L_\perp + d)$ in the bias range $V_c^- < V < V_c^+$ should be calculated from the free energy (15b) as $E_b(V) = \Delta G(P_V^+, V) - \Delta G(P_V^-, V)$. Free energy $\Delta G(P_V)$ calculated from Eq. (15b) for different bias V

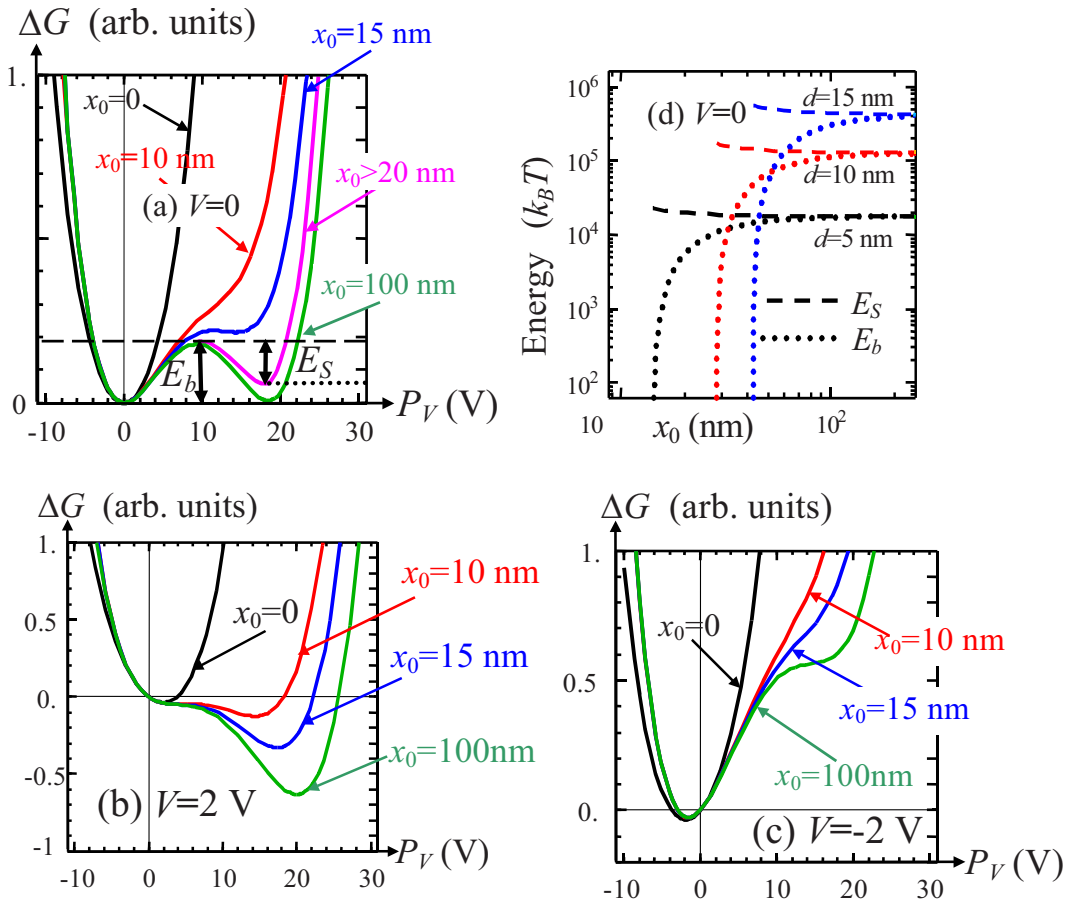

FIG. 8. (Color online) (a), (b), and (c) Free-energy excess ΔG related to the polarization redistribution caused by the probe electric field vs the polarization amplitude P_V (in volts) at different applied bias $V=0$ (a), 2V (b), and −2 V (c). (d) Polarization orientation barrier E_b of nascent domain existing in the range of hysteresis (dashed curves) and the energy E_S of metastable saddle point (dotted curves) vs the distance x_0 between the domain wall and probe apex for fixed charge-surface separation $d=5$, 10, 15 nm (marked near the curves) and $V=0$. Material parameters of $LiNbO_3$ are the same as in Fig. 5.

are shown in Figs. 8(a)–8(c). Orientation barriers via the distance x_0 from domain wall are shown in Fig. 8(d) for different charge-surface separation d.

Within direct variational method the nonlinear behavior of polarization was approximately described by substitution of linearized solution of GLD equation into the free energy with nonlinear terms. This allows us to obtain relatively simple analytical expressions for domain-wall surface profile depending on the one variational parameter P_V. However, rigorously speaking, one should estimate the accuracy of the one-parametric trial function. Recent comparison of approximate one-parametric trial function based on two-dimensional-linearized solution of GLD equation with numerical calculations performed by phase-field modeling has shown that the one-parametric trial function works surprisingly well for the description of domain-wall surface broadening.[23] This encourages us to use the present one-parametric trial function for the description of the interaction of a 180°-ferroelectric domain wall with a biased tip, its surface bending near the probe and obtained radius of nucleating domain. For more rigorous analytical calculations of polarization depth profile and length of tip-induced domains, at least two-parametric trial function may be necessary.

V. SUMMARY

We have analyzed in detail the voltage-dependent thermodynamics and geometry of domain wall in the presence of the localized electric field, corresponding to the physical cases of domain-wall dynamics on the presence of biased SPM probe. Linearized solution of Ginzburg-Landau-Devonshire equation for wall profile is valid for small tip biases. The direct variational method allowed extending this analytical solution to the strongly nonlinear case of arbitrary probe biases, providing the full thermodynamic description of the system in terms of a single voltage-dependent scalar potential. In the uniform field case, corresponding to the infinite tip-surface separation, the potential will become the standard GLD potential function in the uniform field. Obtained analytical expressions provide insight on how the equilibrium polarization distribution depends on the wall finite width, correlation and depolarization effects, electrostatic potential distribution of the probe, and ferroelectric material parameters.

Depending on probe parameters and probe-wall separation, the bias dependence of potential can be single valued, corresponding to the activationless domain-wall bending. For larger values of the probe-wall separation, the potential can exhibit bistability, corresponding to ferroelectric hysteresis. The switching between polarization directions $+P_3$ and $-P_3$ defines the thermodynamic coercive bias of tip-induced domain switching affected by the domain wall. We demonstrate that for small tip-surface separations the domain-wall displacement is activationless, corresponding to the wall bending toward or away from the probe. For intermediate separations, the process is affected by depolarization field induced by wall bending, corresponding to thermodynamics nucleation biases reduced relative to bulk values and appearance of significant loop imprint. Finally, for large tip-surface separations, the wall does not affect nucleation below the tip.

This analysis was performed for the case of ferroelectric material with second-order phase transition in the absence of lattice and defect pinning. It can further be extended to incorporation of lattice effects through the introduction of lattice discreteness or periodic pinning potentials.

ACKNOWLEDGMENTS

S.V.K. gratefully acknowledges multiple discussions with A. K. Tagantsev (EPFL). This research (S.V.K.) at Oak Ridge National Laboratory's Center for Nanophase Materials Sciences was sponsored by the Scientific User Facilities Division, Office of Basic Energy Sciences, U.S. Department of Energy. V.G. wishes to gratefully acknowledge the financial support from the National Science Foundation Grants No. DMR-0602986, No. DMR-0512165, No. DMR-0507146, and No. DMR-0820404 and CNMS2007-007, CNMS2008-283, CNMS2008-289 at Oak Ridge National Laboratory. A.N.M. and S.V.S. gratefully acknowledge the financial support from the National Academy of Science of Ukraine Grant No. N 13-07, joint Russian-Ukrainian grant NASU Grant No. N 17-Ukr_a (RFBR Grant No. N 08-02-90434), Ministry of Science and Education of Ukraine Grant No. N GP/F26/042, and CNMS2008-133 at Oak Ridge National Laboratory.

*Corresponding author. morozo@i.com.ua
†Corresponding author. sergei2@ornl.gov

[1] R. Miller and G. Weinreich, Phys. Rev. **117**, 1460 (1960).
[2] Y. Ishibashi, J. Phys. Soc. Jpn. **46**, 1254 (1979).
[3] I. Suzuki and Y. Ishibashi, Ferroelectrics **64**, 181 (1985).
[4] T. J. Yang, V. Gopalan, P. J. Swart, and U. Mohideen, Phys. Rev. Lett. **82**, 4106 (1999).
[5] G. Rosenman, P. Urenski, A. Agronin, Y. Rosenwaks, and M. Molotski, Appl. Phys. Lett. **82**, 103 (2003).
[6] A. L. Kholkin, I. K. Bdikin, V. V. Shvartsman, A. Orlova, D. Kiselev, A. A. Bogomolov, and S. H. Kim, *Local Electromechanical Properties of Ferroelectric Materials for Piezoelectric Applications*, in Scanning-Probe and Other Novel Microscopies of Local Phenomena in Nanostructured Materials, edited by S. V. Kalinin, B. Goldberg, L. M. Eng, and B. D. Huey, MRS Symposia Proceedings No. 838E (Materials Research Society, Warrendale, PA, 2005), O7.6.
[7] P. Paruch, T. Giamarchi, T. Tybell, and J.-M. Triscone, J. Appl. Phys. **100**, 051608 (2006).
[8] S. V. Kalinin, B. J. Rodriguez, S. Jesse, Y. H. Chu, T. Zhao, R. Ramesh, S. Choudhury, L.-Q. Chen, E. A. Eliseev, and A. N. Morozovska, Proc. Natl. Acad. Sci. U.S.A. **104**, 20204 (2007).
[9] S. Jesse, B. J. Rodriguez, S. Choudhury, A. P. Baddorf, I. Vrejoiu, D. Hesse, M. Alexe, E. A. Eliseev, A. N. Morozovska, J. Zhang, L.-Q. Chen, and S. V. Kalinin, Nat. Mater. **7**, 209 (2008).

[10] S. V. Kalinin, S. Jesse, B. J. Rodriguez, Y. H. Chu, R. Ramesh, E. A. Eliseev, and A. N. Morozovska, Phys. Rev. Lett. **100**, 155703 (2008).
[11] M. Molotskii, A. Agronin, P. Urenski, M. Shvebelman, G. Rosenman, and Y. Rosenwaks, Phys. Rev. Lett. **90**, 107601 (2003).
[12] S. V. Kalinin, A. Gruverman, B. J. Rodriguez, J. Shin, A. P. Baddorf, E. Karapetian, and M. Kachanov, J. Appl. Phys. **97**, 074305 (2005).
[13] A. N. Morozovska, S. V. Svechnikov, E. A. Eliseev, S. Jesse, B. J. Rodriguez, and S. V. Kalinin, J. Appl. Phys. **102**, 114108 (2007).
[14] A. N. Morozovska, S. V. Svechnikov, E. A. Eliseev, B. J. Rodriguez, S. Jesse, and S. V. Kalinin, Phys. Rev. B **78**, 054101 (2008).
[15] Y. L. Li, S. Y. Hu, Z. K. Liu, and L.-Q. Chen, Acta Mater. **50**, 395 (2002).
[16] A. S. Sidorkin, *Domain Structure in Ferroelectrics and Related Materials* (Cambridge International Science, Cambridge, England, 2006).
[17] Y.-H. Shin, I. Grinberg, I.-W. Chen, and A. M. Rappe, Nature (London) **449**, 881 (2007).
[18] A. K. Tagantsev and G. Gerra, J. Appl. Phys. **100**, 051607 (2006).
[19] C. H. Woo and Yue Zheng, Appl. Phys. A: Mater. Sci. Process. **91**, 59 (2007).
[20] R. Kretschmer and K. Binder, Phys. Rev. B **20**, 1065 (1979).
[21] V. A. Zhirnov, Zh. Eksp. Teor. Fiz. **35**, 1175 (1959) [Sov. Phys. JETP **8**, 822 (1959)].
[22] W. Cao and L. E. Cross, Phys. Rev. B **44**, 5 (1991).
[23] E. A. Eliseev, A. N. Morozovska, Y. L. Li, L.-Q. Chen, V. Gopalan, and S. V. Kalinin, arXiv:0802.2559 (unpublished).
[24] C.-L. Jia, V. Nagarajan, J.-Q. He, L. Houben, T. Zhao, R. Ramesh, K. Urban, and R. Waser, Nat. Mater. **6**, 64 (2007).
[25] A. S. Sidorkin, Ferroelectrics **150**, 313 (1993).
[26] M. Molotskii and M. Shvebelman, Philos. Mag. **85**, 1637 (2005).
[27] A. N. Morozovska, S. V. Kalinin, E. A. Eliseev, V. Gopalan, and S. V. Svechnikov, arXiv:0806.2115 (unpublished).
[28] R. K. Dodd, J. C. Eilbeck, J. D. Gibbon, and H. C. Morris, *Solitons and Nonlinear Wave Equations* (Academic, London, 1984), p. 694.
[29] A. N. Morozovska, E. A. Eliseev, and M. D. Glinchuk, Phys. Rev. B **73**, 214106 (2006).
[30] M. D. Glinchuk, E. A. Eliseev, V. A. Stephanovich, and R. Farhi, J. Appl. Phys. **93**, 1150 (2003).